chemistry

MDPI

Article

Remarkably Efficient [4+4] Dimerization of [*n*]-Cyclacenes

Ankit Somani, Divanshu Gupta and Holger F. Bettinger *

Institut für Organische Chemie, Eberhard Karls Universität Tübingen, Auf der Morgenstelle 18, 72076 Tübingen, Germany; ankit.somani@uni-tuebingen.de (A.S.); divanshu.gupta@orgchem.uni-tuebingen.de (D.G.)
* Correspondence: holger.bettinger@uni-tuebingen.de

Abstract: Cyclacenes with the general formula $C_{4n}H_{2n}$ are cyclic analogs of acenes. Acenes are well-known for their high reactivity, which increases with the number of fused benzene rings. The cyclic strain, absence of a Clar sextet, and diradical or polyradical nature are expected to render cyclacenes highly reactive under ambient conditions. Their primary decomposition pathway is anticipated to involve dimerization or polymerization. We explore the reaction pathway of the [$_\pi4_s$ + $_\pi4_s$] dimerization of [*n*]-cyclacenes for $6 \leq n \leq 20$ by density functional theory (DFT) using spin-unrestricted and thermally-assisted-occupation (TAO) formalisms. Computational analysis predicts a stepwise reaction mechanism that starts with the formation of a van der Waals complex and proceeds through a transition state to an intermediate with a single new C–C bond and two unsaturated valences. A subsequent second transition state results in the formation of the dimerization product. However, for smaller cyclacenes ($n < 10$), neither the van der Waals complex nor the first transition state is involved, and the intermediate is formed without a barrier. The largest [20]-cyclacene investigated exhibits the highest barriers for these processes. However, with a barrier as low as 3.9 kcal/mol at the UB3LYP-D3(BJ)/6-31G(d) level of theory, dimerization is anticipated to occur very rapidly.

Keywords: nanorings; nanohoops; density functional theory; forbidden reaction; 4+4 cycloaddition

check for updates

Academic Editors: Takashi Kubo, Yasutaka Kitagawa and Manabu Abe

Received: 27 February 2025
Revised: 7 April 2025
Accepted: 8 April 2025
Published: 12 April 2025

Citation: Somani, A.; Gupta, D.; Bettinger, H.F. Remarkably Efficient [4+4] Dimerization of [*n*]-Cyclacenes. *Chemistry* **2025**, *7*, 62. https://doi.org/10.3390/chemistry7020062

Copyright: © 2025 by the authors. Licensee MDPI, Basel, Switzerland. This article is an open access article distributed under the terms and conditions of the Creative Commons Attribution (CC BY) license (https://creativecommons.org/licenses/by/4.0/).

1. Introduction

Cyclacenes, cyclic analogs of acenes, are a fascinating class of organic molecules consisting of fused benzene rings arranged in a cyclic, belt-like structure (Figure 1) [1]. These molecules are considered part of the nanocarbon family, which includes other well-known carbon-based nanostructures such as graphene, fullerenes, and carbon nanotubes [2,3]. Like acenes [4–14], cyclacenes, with their continuous conjugated π-electron system, are theorized to possess distinctive electronic and optical properties [15–19]. Their unique topology situates them within the field of nanotechnology, offering potential applications in molecular electronics, sensors, and quantum materials [20].

In 1954, Heilbronner introduced the concept of hoop-shaped cyclacene structures [21]. Cyclacenes have been of interest for decades due to their predicted instability under ambient conditions [2]. These organic compounds are anticipated to exhibit a strong tendency to react with their environment, owing to the absence of a Clar sextet and their diradical (or polyradical) character [18,22–24]. The synthesis of [*n*]-cyclacenes remains a major challenge due to their highly strained structures and anticipated high reactivity, resulting in numerous unsuccessful attempts [2,3,25]. However, various carbon nanobelts have been synthesized featuring fused sections that resemble cyclacene structures, such as [12]-, [16]-,

and [24]-membered rings, by Itami and coworkers [26,27]. These nanobelts offer valuable insights into synthetic strategies for cyclacene-like molecules.

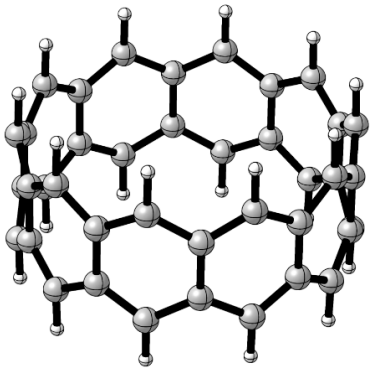


Figure 1. Structure of [10]-cyclacene.

Despite the challenges in directly synthesizing [n]-cyclacenes, significant progress has been made through the synthesis of precursor molecules and derivatives [2,3,28–30]. Key contributions include Stoddart's work on [12]-cyclacene [25,31–34], Cory's efforts on [8]-cyclacene [35,36], and Schlüter's investigations into [18]-cyclacene [37,38]. Wang and colleagues reported the formation of [8]-cyclacene via a retro-Diels–Alder reaction by laser irradiation under mass spectrometry conditions [39]. The attempt to generate [12]-cyclacene on a surface by Gross, Peña, and colleagues was unsuccessful [40].

Here, we report a computational study aimed at understanding the reactivity of [n]-cyclacenes ($6 \leq n \leq 20$) by exploring the mechanism and in particular the barriers of their thermal dimerization. In our previous study of the dimerization of [n]-cyclacene ($6 \leq n \leq 20$), it was found that the dimerization is an extremely exothermic process [41]. The dimerization becomes less exothermic with the increasing size of n, but this change is not monotonic for the smaller members of the series. This is a result of the combination of the cryptoannulenic effect [42–45] and the inherent strain [46–51] of the cyclacenes.

The dimerization reaction can be viewed as an orbital symmetry-forbidden [$_{\pi}4_{s}$ + $_{\pi}4_{s}$] cycloaddition; hence, it is expected that the mechanism is stepwise involving a diradical-type intermediate with two unsaturated valences as it is known to be the case for acenes [52]. Due to strong static correlation effects inherent to [n]-cyclacenes [17,18,46,53,54], traditional electronic structure methods often face significant limitations in accurately describing their electronic properties [55]. To address these challenges, we employ unrestricted hybrid Kohn–Sham density functional theory (KS-DFT) methods [56], along with thermally-assisted-occupation density functional theory (TAO-DFT) [18,19,24,57,58]. TAO-DFT is particularly suited to handle large systems with strong static correlation effects as it leverages fractional orbital occupations and incorporates an entropy term that effectively lowers the total energy in multi-reference systems, enabling a more accurate and computationally efficient analysis.

2. Methods

All the structures were fully optimized using density functional theory [59,60] (DFT) with the spin-unrestricted B3LYP [61,62] hybrid exchange-correlation energy functional, along with Grimme's [63] London dispersion correction with Becke–Johnson damping UB3LYP-D3(BJ) [64]. The 6-31G(d) basis set was adopted for all computations reported in this work [65]. All Gibbs free energy values (Table S3) are at T = 298.15 K, p = 1 atm. Harmonic vibrational frequencies were computed analytically, which confirmed the nature of the stationary points as minima, or first-order saddle points (transition states). Additionally, to reveal which minima are connected to the transition states, intrinsic reaction

coordinate (IRC) paths were calculated at the UB3LYP-D3(BJ) level of theory for each reaction [66,67]. In addition, the geometry of stationary points was also fully optimized using the UM06-2X [68] functional in conjunction with the 6-31G(d) basis set. The UB3LYP-D3(BJ) geometries were employed for subsequent single-point energies using UB3LYP and TAO-B3LYP [57] without and with D3 London dispersion correction to evaluate the impact of London dispersion on the potential energy surfaces. The expectation values of the $\hat{S}^2$ operator are given in the SI (Table S6). The UB3LYP and UM06-2X computations were performed with Gaussian 16 [69], while TAO-B3LYP was performed with Q-Chem 6.2 [70]. The default parameters of Q-Chem were employed in our study. The TAO-B3LYP runs emplyod a numerical grid containing 75 radial points in the Euler–Maclaurin quadrature and 302 angular points in the Lebedev grid. Unless mentioned otherwise, the UB3LYP-D3(BJ) results are presented in the manuscript, while the UB3LYP, UM06-2X, TAO-B3LYP, and TAO-B3LYP-D3 data can be found in the Supporting Information. Natural orbital occupation numbers were computed (Table S7) using geometries optimized at the UB3LYP-D3(BJ)/6-31G(d) level of theory. Fractional occupation number-weighted density (FOD) [71,72] calculations (Table S8) were carried out with ORCA 5.0.1 [73,74] at the TPSS/def2-TZVP [75,76] level at a default electronic temperature (T_{el}) of 5000 K using UB3LYP-D3(BJ)/6-31G(d) geometries.

3. Results and Discussion

Given the diradical or polyradical nature of [*n*]-cyclacenes, this study employs a spin-unrestricted treatment with B3LYP functional. As emphasized in our previous work [41], the dimerization of [*n*]-cyclacenes is highly exothermic, highlighting their thermodynamic instability despite some aromatic character (Figure 2) [15,16,77].

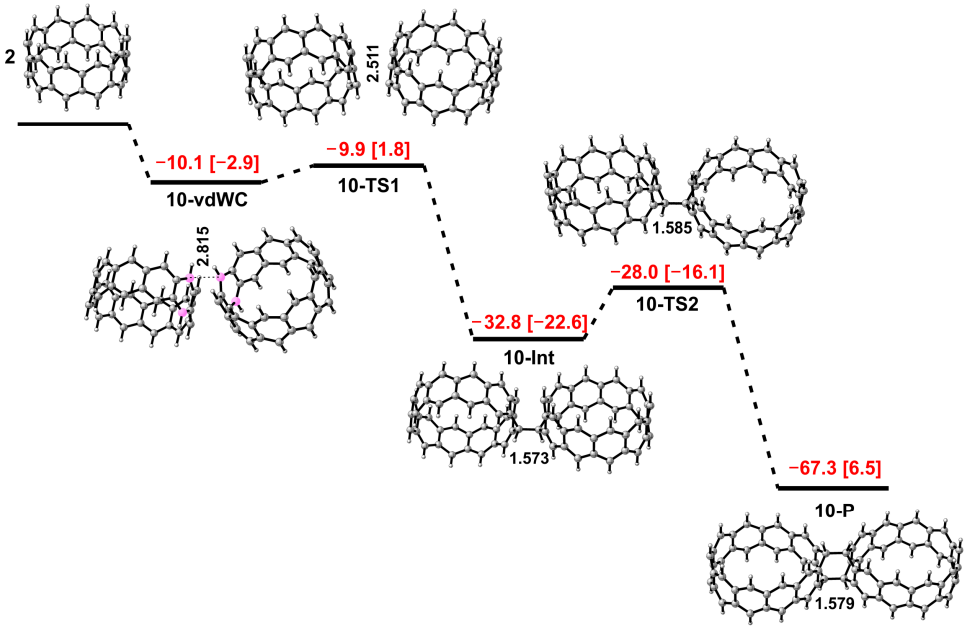


Figure 2. Reaction path for dimerization of [10]-cyclacene. Calculated ZPVE corrected relative energies (in kcal/mol, red) and bond lengths of newly forming C–C bonds (in Å, black) at the UB3LYP-D3(BJ)/6-31G(d) level of theory are shown. The Gibbs free energy (Δ*G*, in kcal/mol) values are given in brackets. Carbon atoms defining the dihedral angle are highlighted in the 10-vdWC structure.

The computational analysis reveals that the reaction proceeds via a stepwise mechanism involving an intermediate with two unsaturated valences (formally a diradical). The dimerization reaction of [*n*]-cyclacenes ($10 \leq n \leq 20$) begins with the formation of a van der Waals complex (vdWC) between two [*n*]-cyclacene molecules. Note that the vdWC (and the associated transition state for the formation of the intermediate) is not observed for smaller

cyclacenes ($n < 10$) (see below for further discussion). At the UB3LYP-D3(BJ)/6-31G(d) level of theory, the complex (10-vdWC), with a separation of 2.815 Å and a dihedral angle of 72.9°, is approximately 10.1 kcal/mol more stable than the reactants for [10]-cyclacene (Figure 2). The dihedral angle between the two interacting rings of [*n*]-cyclacene decreases as the size of the cyclacene increases, with the smallest angle, approximately 46.5°, observed in the vdWC of [20]-cyclacene dimerization. The intermolecular distance between the two closest carbon atoms in the complex shows an increase with increasing size of the cyclacene (Figure S5).

As the cyclacene size increases, the formation of vdWC becomes more exothermic. However, the change is relatively small, varying by approximately 3.1 kcal/mol from [10]- to [20]-cyclacene (Table S1, Figure 3). The single-point energies computed at the TAO-B3LYP-D3/6-31G(d) level of theory, using geometries optimized at the UB3LYP-D3(BJ)/6-31G(d) level, are lowered by approximately 1 kcal/mol, indicating the effectiveness of the spin-unrestricted approach with B3LYP. At the UM06-2X/6-31G(d) level of theory, a similar pattern is observed in the relative energy of the complex (*n*-vdWC); however, it remains consistently higher by approximately 3–4 kcal/mol compared to that at the UB3LYP-D3(BJ)/6-31G(d) level of theory (Table S1).

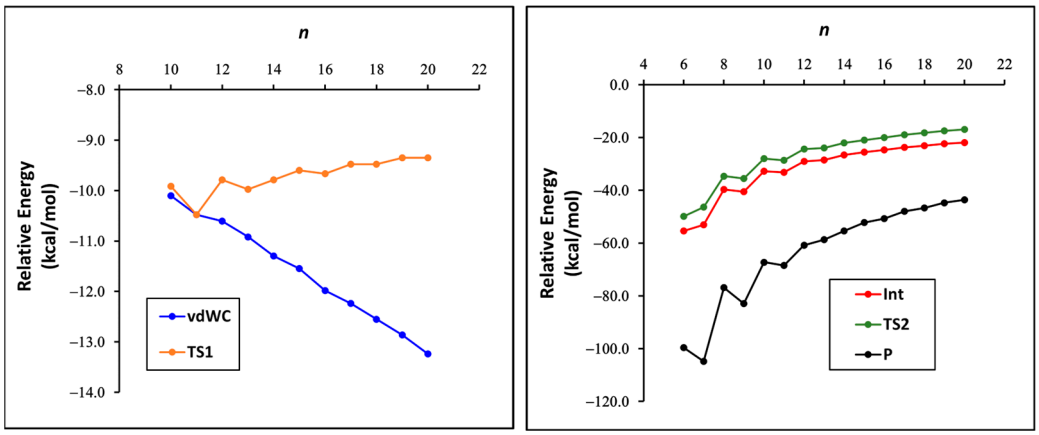


Figure 3. Dependence of computed energies relative to two cyclacene molecules of vdWC, TS1, Int, TS2, and dimer (UB3LYP-D3(BJ)/6-31G(d)) on cyclacene size.

The reaction proceeds via a transition state (10-TS1) with an extremely small activation barrier of only 0.2 kcal/mol at the UB3LYP-D3(BJ)/6-31G(d) level of theory, leading to an intermediate (10-Int) characterized by the formation of a C–C bond between the two cyclacene molecules. The activation barrier shows a monotonic increase with the increasing size of the cyclacene (Figure 3). The highest barrier calculated is 3.9 kcal/mol for [20]-cyclacene. Since the single-point energies calculated for the vdWC and TS1 at the TAO-B3LYP-D3/6-31G(d)//UB3LYP-D3(BJ)/6-31G(d) level of theory are lowered by a similar amount (~1 kcal/mol), the activation barriers are consequently calculated to be similar. The distance in TS1 ($10 \leq n \leq 20$) between the two carbon atoms involved in the C–C bond formation decreases with increasing cyclacene size, in contrast to what we observe in the complex (Figure S5). The dihedral angle of TS1 decreases continuously from 70.0° for [10]-cyclacene to 53.3° for [20]-cyclacene (Table S4). A similar trend is observed in the intermediate (n-Int) featuring the newly formed C–C bond. However, in contrast to TS1, the C–C bond length in the intermediate increases with the size of the cyclacene.

The reaction then proceeds through a second transition state TS2, involving the rotation of the two cyclacene moieties to reduce the dihedral angle further, ultimately leading to the final product (10-P) with a dihedral angle of 0°. At the UB3LYP-D3(BJ)/6-31G(d) level of theory, the activation barrier for larger [*n*]-cyclacenes ($10 \leq n \leq 20$) is calculated to

be approximately 4.5–5 kcal/mol. The activation barrier is slightly higher for smaller [n]-cyclacenes ($6 \leq n \leq 9$), ranging from 5–7 kcal/mol. In contrast, the activation barrier remains approximately 4.5–5 kcal/mol for [n]-cyclacene ($6 \leq n \leq 20$) calculated at the TAO-B3LYP-D3/6-31G(d)//UB3LYP-D3(BJ)/6-31G(d) level of theory. The relative energies of the intermediate, TS2, and the final product, calculated at the UM06-2X/6-31G(d) level of theory, follow the same pattern as those at the UB3LYP-D3(BJ)/6-31G(d) level, as seen for the complex and TS1. However, in this case, the relative energies of the intermediate, TS2, and the dimer are calculated to be lower (Table S1).

For smaller [n]-cyclacenes ($6 \leq n \leq 9$), the complex (n-vdWC) and first transition state (n-TS1) could not be obtained as stationary points; therefore, the reaction proceeds by direct formation of the intermediate (n-Int) (Figure 4). We suspect that this higher reactivity of smaller cyclacenes is due to their increased strain. The relative energies of the intermediate and second transition states exhibit an oscillatory behavior for smaller cyclacenes ($6 \leq n \leq 11$) and, subsequently, show a monotonic change, as observed in the dimerization energy with an exception in the case of [7]-cyclacene (Figure 3). The two identical C–C bonds formed in the final dimer product between two cyclacene molecules show an increase in the bond length with the increasing size of the cyclacene. For a detailed comparison of the distance between two cyclacene units in the stationary points, see Figure S5.

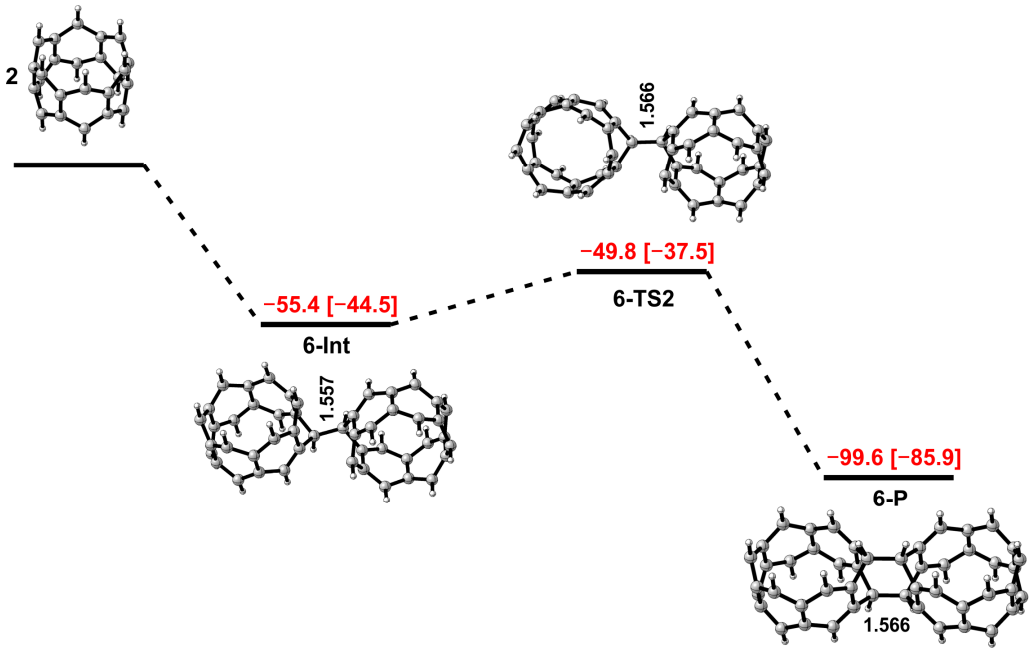


Figure 4. Reaction path for dimerization of [6]-cyclacene. Calculated ZPVE corrected relative energies (in kcal/mol, red) and bond length of newly forming C–C bonds (in Å, black) at UB3LYP-D3(BJ)/6-31G(d) level of theory are shown. The Gibbs free energy (ΔG, in kcal/mol) values are given in brackets.

The mechanism that we have elucidated in the present work resembles that of acene dimerization that has previously been studied computationally by Bendikov and co-workers at M06-2X/6-31G(d) + ZPVE [52,78]. Dimerization of heptacene, the largest acene investigated [52], likewise begins with the exothermic (−24.4 kcal/mol) formation of a complex between two heptacene molecules. The formation of the diradical intermediate from the complex has an activation barrier of 12.3 kcal/mol. In comparison, for [7]-cyclacene, neither the 7-vdWC nor 7-TS1 was identified; therefore, the reaction proceeds

via the direct formation of the intermediate (7-Int), indicating extremely high reactivity towards dimerization.

Heptacene, in solution, is known to dimerize under ambient conditions [79] in accordance with the low barrier for dimerization [52]. In the solid state, heptacene and nonacene can be obtained as metastable materials, presumably because the dimerization causes a significant structural change that would cause local strain in the solid [79,80]. The diradical intermediate that is involved in the dimerization of heptacene could recently be detected by EPR spectroscopy in a solid sample of heptacene and was found to have a singlet ground state with a very small singlet–triplet energy gap of -4.8×10^{-3} kcal/mol [81]. It is likely that barriers of around 5 kcal/mol that are computed for the final formation of cyclacenes would similarly allow for the detection of the intermediate for cyclacene dimerization.

Finally, we note that [*n*]-cyclacenes were identified as being able to sustain ring currents [15,16,77]. Based on magnetic criteria such as nucleus-independent chemical shift (NICS), diamagnetic susceptibility exaltation, and anisotropy of the induced current density (ACID), it was concluded that even-*n* cyclacenes are aromatic, while odd-*n* cyclacenes are non-aromatic or weakly antiaromatic [15,16,77]. We observe no enhanced kinetic stability of the even-*n* over the odd-*n* cyclacenes in the computed barrier heights (Figure S1). The very small barriers for dimerization suggest that the aromaticity based on magnetic criteria cannot endow the systems with the kinetic stability that is typically associated with aromaticity. It appears that strain, rather than aromaticity, controls their reactivity.

4. Conclusions

Our computational investigation of the dimerization mechanism of [*n*]-cyclacenes reveals that these molecules are highly reactive. The analysis suggests that the reaction follows a stepwise mechanism as expected for a [$_{\pi}4_{s}$ + $_{\pi}4_{s}$] cycloaddition reaction that is thermally orbital symmetry forbidden. Cyclacenes have very low activation barriers for dimerization, regardless of their size, and are thus expected to display a strong tendency to dimerize. The reaction sets in with the formation of an energetically favorable complex between two [*n*]-cyclacene molecules for $n > 10$. This is followed by a facile (activation barrier < 4 kcal/mol) formation of one C—C single bond between the two molecules of cyclacenes, yielding a diradical-type intermediate with two unsaturated valences. The reaction then proceeds through a second transition state, with an activation barrier of 4–7 kcal/mol, which reduces the dihedral angle between the two cyclacene moieties, ultimately resulting in the dimeric product. We do not find evidence that even-n cyclacenes would be stabilized by the aromaticity that was identified previously based on magnetic criteria [15,16,77].

Supplementary Materials: The following supporting information can be downloaded at https://www.mdpi.com/article/10.3390/chemistry7020062/s1: Computed relative energies and relative Gibbs free energies of all the molecules at different levels of theory. Graphical representation of activation barriers for TS1, TS2, and their corresponding IRCs. Bond lengths and dihedral angles of newly formed C–C bond. $\hat{S}^2$ operator expectation values, natural orbital occupancy numbers, and FOD numbers for all molecules. Cartesian coordinates for all stationary points.

Author Contributions: Conceptualization, H.F.B.; methodology, A.S., D.G. and H.F.B.; validation, A.S., D.G. and H.F.B.; investigation, A.S. and D.G.; resources, H.F.B.; data curation, A.S. and D.G.; writing—original draft preparation, A.S.; writing—review and editing, D.G. and H.F.B.; visualization, A.S. and D.G.; supervision, H.F.B.; project administration, H.F.B.; funding acquisition, H.F.B. All authors have read and agreed to the published version of the manuscript.

Funding: This project has received funding from the European Research Council (ERC) under the European Union's HORIZON ERC Synergy Grants action via the project Tackling the Cyclacene

Challenge (TACY), grant agreement number: 101071420-TACY-ERC-2022-SYG. The computations were performed on the BwForCluster JUSTUS2 cluster. The authors acknowledge support by the state of Baden-Württemberg through bwHPC and the German Research Foundation (DFG) through grant no. INST 40/575-1 FUGG (JUSTUS 2 cluster) for computation facilities.

Data Availability Statement: Relevant data is provided as part of Supplementary Materials.

Conflicts of Interest: The authors declare no conflict of interest.

References

1. Türker, L.; Gümüş, S. Cyclacenes. *J. Mol. Struct. THEOCHEM* **2004**, *685*, 1–33. [CrossRef]
2. Gleiter, R.; Esser, B.; Kornmayer, S.C. Cyclacenes: Hoop-Shaped Systems Composed of Conjugated Rings. *Acc. Chem. Res.* **2009**, *42*, 1108–1116. [CrossRef] [PubMed]
3. Shi, T.-H.; Wang, M.-X. Zigzag Hydrocarbon Belts. *CCS Chem.* **2021**, *3*, 916–931. [CrossRef]
4. Bendikov, M.; Duong, H.M.; Starkey, K.; Houk, K.N.; Carter, E.A.; Wudl, F. Oligoacenes: Theoretical Prediction of Open-Shell Singlet Diradical Ground States. *J. Am. Chem. Soc.* **2004**, *126*, 7416–7417. [CrossRef]
5. Hachmann, J.; Dorando, J.J.; Avilés, M.; Chan, G.K.-L. The radical character of the acenes: A density matrix renormalization group study. *J. Chem. Phys.* **2007**, *127*, 13. [CrossRef] [PubMed]
6. Jiang, D.-e.; Dai, S. Electronic Ground State of Higher Acenes. *J. Phys. Chem. A* **2008**, *112*, 332–335. [CrossRef]
7. Bettinger, H.F. Electronic structure of higher acenes and polyacene: The perspective developed by theoretical analyses. *Pure Appl. Chem.* **2010**, *82*, 905–915. [CrossRef]
8. Yang, Y.; Davidson, E.R.; Yang, W. Nature of ground and electronic excited states of higher acenes. *Proc. Natl. Acad. Sci. USA* **2016**, *113*, E5098–E5107. [CrossRef]
9. Urgel, J.I.; Mishra, S.; Hayashi, H.; Wilhelm, J.; Pignedoli, C.A.; Di Giovannantonio, M.; Widmer, R.; Yamashita, M.; Hieda, N.; Ruffieux, P.; et al. On-surface light-induced generation of higher acenes and elucidation of their open-shell character. *Nat. Commun.* **2019**, *10*, 861. [CrossRef]
10. Tönshoff, C.; Bettinger, H.F. Pushing the limits of acene chemistry: The recent surge of large acenes. *Chem. Eur. J.* **2021**, *27*, 3193–3212. [CrossRef]
11. Lerena, L.; Zuzak, R.; Godlewski, S.; Echavarren, A.M. The Journey for the Synthesis of Large Acenes. *Chem. Eur. J.* **2024**, *30*, e202402122. [CrossRef] [PubMed]
12. Ruan, Z.; Schramm, J.; Bauer, J.B.; Naumann, T.; Bettinger, H.F.; Tonner-Zech, R.; Gottfried, J.M. Synthesis of Tridecacene by Multistep Single-Molecule Manipulation. *J. Am. Chem. Soc.* **2024**, *146*, 3700–3709. [CrossRef] [PubMed]
13. Zuzak, R.; Kumar, M.; Stoica, O.; Soler-Polo, D.; Brabec, J.; Pernal, K.; Veis, L.; Blieck, R.; Echavarren, A.M.; Jelinek, P.; et al. On-Surface Synthesis and Determination of the Open-Shell Singlet Ground State of Tridecacene. *Angew. Chem. Int. Ed.* **2024**, *63*, e202317091. [CrossRef] [PubMed]
14. Ruan, Z.; Schramm, J.; Bauer, J.B.; Naumann, T.; Müller, L.V.; Sättele, F.; Bettinger, H.F.; Tonner-Zech, R.; Gottfried, J.M. On-Surface Synthesis and Characterization of Pentadecacene and Its Gold Complexes. *J. Am. Chem. Soc.* **2025**, *147*, 4862–4870. [CrossRef]
15. Türker, L. The Possibility of Superaromatic Cyclacenes. *Polycyclic Aromat. Compd.* **1995**, *4*, 231–236. [CrossRef]
16. Choi, H.S.; Kim, K.S. Structures, Magnetic Properties, and Aromaticity of Cyclacenes. *Angew. Chem. Int. Ed.* **1999**, *38*, 2256–2258. [CrossRef]
17. Chen, Z.; Jiang, D.-e.; Lu, X.; Bettinger, H.F.; Dai, S.; Schleyer, P.v.R.; Houk, K.N. Open-Shell Singlet Character of Cyclacenes and Short Zigzag Nanotubes. *Org. Lett.* **2007**, *9*, 5449–5452. [CrossRef]
18. Wu, C.-S.; Lee, P.-Y.; Chai, J.-D. Electronic Properties of Cyclacenes from TAO-DFT. *Sci. Rep.* **2016**, *6*, 37249. [CrossRef]
19. Chung, J.-H.; Chai, J.-D. Electronic Properties of Möbius Cyclacenes Studied by Thermally-Assisted-Occupation Density Functional Theory. *Sci. Rep.* **2019**, *9*, 2907. [CrossRef]
20. Huang, X.; Gan, P.-y.; Gao, F.-w.; Su, Z.-m. Tuning optical properties of π-conjugated double nanohoops under external electric field stimuli-responsiveness. *Phys. Chem. Chem. Phys.* **2024**, *26*, 8716–8723. [CrossRef]
21. Heilbronner, E. Molecular Orbitals in homologen Reihen mehrkerniger aromatischer Kohlenwasserstoffe: I. Die Eigenwerte yon LCAO-MO's in homologen Reihen. *Helv. Chim. Acta* **1954**, *37*, 921–935. [CrossRef]
22. Clar, E. The Aromatic Sextet. In *Mobile Source Emissions Including Policyclic Organic Species*; Rondia, D., Cooke, M., Haroz, R.K., Eds.; Springer: Dordrecht, The Netherlands, 1983; pp. 49–58.
23. Solà, M. Forty years of Clar's aromatic π-sextet rule. *Front. Chem.* **2013**, *1*, 22. [CrossRef]
24. Chai, J.-D. Thermally-assisted-occupation density functional theory with generalized-gradient approximations. *J. Chem. Phys.* **2014**, *140*. [CrossRef]
25. Guo, Q.-H.; Qiu, Y.; Wang, M.-X.; Fraser Stoddart, J. Aromatic hydrocarbon belts. *Nat. Chem.* **2021**, *13*, 402–419. [CrossRef]

26. Povie, G.; Segawa, Y.; Nishihara, T.; Miyauchi, Y.; Itami, K. Synthesis of a carbon nanobelt. *Science* **2017**, *356*, 172–175. [CrossRef] [PubMed]
27. Povie, G.; Segawa, Y.; Nishihara, T.; Miyauchi, Y.; Itami, K. Synthesis and Size-Dependent Properties of [12], [16], and [24]Carbon Nanobelts. *J. Am. Chem. Soc.* **2018**, *140*, 10054–10059. [CrossRef]
28. Bauer, J.B.; Diab, F.; Maichle-Mössmer, C.; Schubert, H.; Bettinger, H.F. Synthesis of the [11]Cyclacene Framework by Repetitive Diels–Alder Cycloadditions. *Molecules* **2021**, *26*, 3047. [CrossRef] [PubMed]
29. Eisenberg, D.; Shenhar, R.; Rabinovitz, M. Synthetic approaches to aromatic belts: Building up strain in macrocyclic polyarenes. *Chem. Soc. Rev.* **2010**, *39*, 2879–2890. [CrossRef]
30. Chen, H.; Gui, S.; Zhang, Y.; Liu, Z.; Miao, Q. Synthesis of a Hydrogenated Zigzag Carbon Nanobelt. *CCS Chem.* **2021**, *3*, 613–619. [CrossRef]
31. Kohnke, F.H.; Slawin, A.M.; Stoddart, J.F.; Williams, D.J. Molecular belts and collars in the making: A hexaepoxyoctacosahydro [12] cyclacene derivative. *Angew. Chem. Int. Ed.* **1987**, *26*, 892–894. [CrossRef]
32. Ashton, P.R.; Isaacs, N.S.; Kohnke, F.H.; Slawin, A.M.; Spencer, C.M.; Stoddart, J.F.; Williams, D.J. Towards the making of [12] collarene. *Angew. Chem. Int. Ed.* **1988**, *27*, 966–969. [CrossRef]
33. Ashton, P.R.; Brown, G.R.; Isaacs, N.S.; Giuffrida, D.; Kohnke, F.H.; Mathias, J.P.; Slawin, A.M.Z.; Smith, D.R.; Stoddart, J.F.; Williams, D.J. Molecular LEGO. 1. Substrate-directed synthesis via stereoregular Diels-Alder oligomerizations. *J. Am. Chem. Soc.* **1992**, *114*, 6330–6353. [CrossRef]
34. Ashton, P.R.; Girreser, U.; Giuffrida, D.; Kohnke, F.H.; Mathias, J.P.; Raymo, F.M.; Slawin, A.M.; Stoddart, J.F.; Williams, D.J. Molecular belts. 2. Substrate-directed syntheses of belt-type and cage-type structures. *J. Am. Chem. Soc.* **1993**, *115*, 5422–5429. [CrossRef]
35. Cory, R.M.; McPhail, C.L. Transformations of a macrocyclic cyclophane belt into advanced [8] cyclacene and [8] cyclacene triquinone precursors. *Tetrahedron Lett.* **1996**, *37*, 1987–1990. [CrossRef]
36. Cory, R.M.; McPhail, C.L.; Dikmans, A.J.; Vittal, J.J. Macrocyclic cyclophane belts via double Diels-Alder cycloadditions: Macroannulation of bisdienes by bisdienophiles. Synthesis of a key precursor to an [8] cyclacene. *Tetrahedron Lett.* **1996**, *37*, 1983–1986. [CrossRef]
37. Godt, A.; Enkelmann, V.; Schlüter, A.D. Double-Stranded Molecules: A [6] Beltene Derivative and the Corresponding Open-Chain Polymer. *Angew. Chem. Int. Ed.* **1989**, *28*, 1680–1682. [CrossRef]
38. Kintzel, O.; Luger, P.; Weber, M.; Schlüter, A.-D. Ring-Chain Equilibrium between an [18]Cyclacene Derivative and a Ladder Oligomer. *Eur. J. Org. Chem.* **1998**, *1998*, 99–105. [CrossRef]
39. Shi, T.-H.; Guo, Q.-H.; Tong, S.; Wang, M.-X. Toward the Synthesis of a Highly Strained Hydrocarbon Belt. *J. Am. Chem. Soc.* **2020**, *142*, 4576–4580. [CrossRef]
40. Schulz, F.; García, F.; Kaiser, K.; Pérez, D.; Guitián, E.; Gross, L.; Peña, D. Exploring a Route to Cyclic Acenes by On-Surface Synthesis. *Angew. Chem. Int. Ed.* **2019**, *58*, 9038–9042. [CrossRef]
41. Somani, A.; Gupta, D.; Bettinger, H.F. Computational Studies of Dimerization of [n]-Cyclacenes. *J. Phys. Chem. A* **2024**, *128*, 6847–6852. [CrossRef]
42. Türker, L. Cryptoannulenic Behavior of Cyclacenes. *Polycyclic Aromat. Compd.* **1994**, *4*, 191–197. [CrossRef]
43. Türker, L. AM1 treatment of Hückel type cyclacenes. *J. Mol. Struct.* **1997**, *407*, 217–220. [CrossRef]
44. Türker, L. MNDO treatment of the Hückel and Möbius types of cyclacenes. *J. Mol. Struct. THEOCHEM* **1998**, *454*, 83–86. [CrossRef]
45. Türker, L. The Effect of Peripheral Circuits on the Total\pi-Electron Energies of Cyclacenes. *Turk. J. Chem.* **2000**, *24*, 217–222.
46. Sadowsky, D.; McNeill, K.; Cramer, C.J. Electronic structures of [n]-cyclacenes (n = 6–12) and short, hydrogen-capped, carbon nanotubes. *Faraday Discuss.* **2010**, *145*, 507–521. [CrossRef]
47. Christoph, H.; Grunenberg, J.; Hopf, H.; Dix, I.; Jones, P.G.; Scholtissek, M.; Maier, G. MP2 and DFT Calculations on Circulenes and an Attempt to Prepare the Second Lowest Benzolog, [4]Circulene. *Chem. Eur. J.* **2008**, *14*, 5604–5616. [CrossRef]
48. Gupta, D.; Omont, A.; Bettinger, H.F. Energetics of Formation of Cyclacenes from 2,3-Didehydroacenes and Implications for Astrochemistry. *Chem. Eur. J.* **2021**, *27*, 4605–4616. [CrossRef]
49. Segawa, Y.; Omachi, H.; Itami, K. Theoretical Studies on the Structures and Strain Energies of Cycloparaphenylenes. *Org. Lett.* **2010**, *12*, 2262–2265. [CrossRef]
50. Segawa, Y.; Yagi, A.; Ito, H.; Itami, K. A Theoretical Study on the Strain Energy of Carbon Nanobelts. *Org. Lett.* **2016**, *18*, 1430–1433. [CrossRef]
51. Smith, P.J.; Liebman, J.F.; Hopf, H.; Starý, I.; Stará, I.G.; Halton, B. Strained Aromatic Molecules. In *Strained Hydrocarbons*; Wiley-VCH Verlag GmbH & Co. KGaA: Weinheim, Germany, 2009; pp. 147–204.
52. Zade, S.S.; Zamoshchik, N.; Reddy, A.R.; Fridman-Marueli, G.; Sheberla, D.; Bendikov, M. Products and mechanism of acene dimerization. A computational study. *J. Am. Chem. Soc.* **2011**, *133*, 10803–10816. [CrossRef]

53. Battaglia, S.; Faginas-Lago, N.; Andrae, D.; Evangelisti, S.; Leininger, T. Increasing Radical Character of Large [n]cyclacenes Unveiled by Wave Function Theory. *J. Phys. Chem. A* **2017**, *121*, 3746–3756. [CrossRef]
54. Pérez-Guardiola, A.; Sandoval-Salinas, M.E.; Casanova, D.; San-Fabián, E.; Pérez-Jiménez, A.J.; Sancho-García, J.C. The role of topology in organic molecules: Origin and comparison of the radical character in linear and cyclic oligoacenes and related oligomers. *Phys. Chem. Chem. Phys.* **2018**, *20*, 7112–7124. [CrossRef] [PubMed]
55. Cohen, A.J.; Mori-Sánchez, P.; Yang, W. Challenges for Density Functional Theory. *Chem. Rev.* **2012**, *112*, 289–320. [CrossRef] [PubMed]
56. Kohn, W.; Sham, L.J. Self-Consistent Equations Including Exchange and Correlation Effects. *Phys. Rev.* **1965**, *140*, A1133–A1138. [CrossRef]
57. Chai, J.-D. Role of exact exchange in thermally-assisted-occupation density functional theory: A proposal of new hybrid schemes. *J. Chem. Phys.* **2017**, *146*. [CrossRef]
58. Chen, B.-J.; Chai, J.-D. TAO-DFT fictitious temperature made simple. *RSC Adv.* **2022**, *12*, 12193–12210. [CrossRef]
59. Koch, W.; Holthausen, M.C. *A Chemist's Guide to Density Functional Theory*; John Wiley & Sons: Hoboken, NJ, USA, 2015.
60. Parr, R.G. Density functional theory. *Annu. Rev. Phys. Chem.* **1983**, *34*, 631–656. [CrossRef]
61. Lee, C.; Yang, W.; Parr, R.G. Development of the Colle-Salvetti correlation-energy formula into a functional of the electron density. *Phys. Rev. B* **1988**, *37*, 785–789. [CrossRef]
62. Becke, A.D. Density-functional thermochemistry. III. The role of exact exchange. *J. Chem. Phys.* **1993**, *98*, 5648–5652. [CrossRef]
63. Grimme, S. Density functional theory with London dispersion corrections. *Wiley Interdiscip. Rev. Comput. Mol. Sci.* **2011**, *1*, 211–228. [CrossRef]
64. Grimme, S.; Ehrlich, S.; Goerigk, L. Effect of the damping function in dispersion corrected density functional theory. *J. Comput. Chem.* **2011**, *32*, 1456–1465. [CrossRef] [PubMed]
65. Ditchfield, R.; Hehre, W.J.; Pople, J.A. Self-Consistent Molecular-Orbital Methods. IX. An Extended Gaussian-Type Basis for Molecular-Orbital Studies of Organic Molecules. *J. Chem. Phys.* **1971**, *54*, 724–728. [CrossRef]
66. Hratchian, H.P.; Schlegel, H.B. Accurate reaction paths using a Hessian based predictor–corrector integrator. *J. Chem. Phys.* **2004**, *120*, 9918–9924. [CrossRef]
67. Hratchian, H.; Schlegel, H. Using Hessian updating to increase the efficiency of a Hessian based predictor-corrector reaction path following method. *J. Chem. Theory Comput.* **2005**, *1*, 61–69. [CrossRef]
68. Zhao, Y.; Truhlar, D.G. The M06 suite of density functionals for main group thermochemistry, thermochemical kinetics, noncovalent interactions, excited states, and transition elements: Two new functionals and systematic testing of four M06-class functionals and 12 other functionals. *Theor. Chem. Acc.* **2008**, *120*, 215–241.
69. Frisch, M.J.; Trucks, G.W.; Schlegel, H.B.; Scuseria, G.E.; Robb, M.A.; Cheeseman, J.R.; Scalmani, G.; Barone, V.; Petersson, G.A.; Nakatsuji, H.; et al. *Gaussian 16 Revision C. 01, 2016*; Gaussian Inc.: Wallingford, CT, USA, 2016; Volume 1, p. 572.
70. Epifanovsky, E.; Gilbert, A.T.; Feng, X.; Lee, J.; Mao, Y.; Mardirossian, N.; Pokhilko, P.; White, A.F.; Coons, M.P.; Dempwolff, A.L. Software for the frontiers of quantum chemistry: An overview of developments in the Q-Chem 5 package. *J. Chem. Phys.* **2021**, *155*, 084801.
71. Grimme, S.; Hansen, A. A Practicable Real-Space Measure and Visualization of Static Electron-Correlation Effects. *Angew. Chem. Int. Ed.* **2015**, *54*, 12308–12313. [CrossRef]
72. Bauer, C.A.; Hansen, A.; Grimme, S. The Fractional Occupation Number Weighted Density as a Versatile Analysis Tool for Molecules with a Complicated Electronic Structure. *Chem. Eur. J.* **2017**, *23*, 6150–6164. [CrossRef]
73. Neese, F. Software update: The ORCA program system—Version 5.0. *WIREs Comput. Mol. Sci.* **2022**, *12*, e1606. [CrossRef]
74. Neese, F. The ORCA program system. *WIREs Comput. Mol. Sci.* **2012**, *2*, 73–78. [CrossRef]
75. Tao, J.; Perdew, J.P.; Staroverov, V.N.; Scuseria, G.E. Climbing the Density Functional Ladder: Nonempirical Meta--Generalized Gradient Approximation Designed for Molecules and Solids. *Phys. Rev. Lett.* **2003**, *91*, 146401. [CrossRef] [PubMed]
76. Weigend, F.; Ahlrichs, R. Balanced basis sets of split valence, triple zeta valence and quadruple zeta valence quality for H to Rn: Design and assessment of accuracy. *Phys. Chem. Chem. Phys.* **2005**, *7*, 3297–3305. [CrossRef] [PubMed]
77. Li, Q.; Xu, H.-L.; Su, Z.-M. NICS values scan in three-dimensional space of the hoop-shaped π-conjugated molecules $[6]_8$cyclacene and [16]trannulene. *New J. Chem.* **2018**, *42*, 1987–1994. [CrossRef]
78. Zamoshchik, N.; Zade, S.S.; Bendikov, M. Formation of Acene-Based Polymers: Mechanistic Computational Study. *J. Org. Chem.* **2013**, *78*, 10058–10068. [CrossRef]
79. Einholz, R.; Fang, T.; Berger, R.; Grüninger, P.; Fruh, A.; Chasse, T.; Fink, R.F.; Bettinger, H.F. Heptacene: Characterization in solution, in the solid state, and in films. *J. Am. Chem. Soc.* **2017**, *139*, 4435–4442. [CrossRef] [PubMed]

80. Jančařík, A.; Holec, J.; Nagata, Y.; Šámal, M.; Gourdon, A. Preparative-scale synthesis of nonacene. *Nat. Commun.* **2022**, *13*, 223. [CrossRef]
81. Wagner, M.S.; Peisert, H.; Chassé, T.; Bettinger, H.F. Detection of diheptacendiyl diradical intermediate in the cycloreversion of diheptacene to heptacene. *Chem. Commun.* **2024**, *60*, 8451–8453. [CrossRef]

Disclaimer/Publisher's Note: The statements, opinions and data contained in all publications are solely those of the individual author(s) and contributor(s) and not of MDPI and/or the editor(s). MDPI and/or the editor(s) disclaim responsibility for any injury to people or property resulting from any ideas, methods, instructions or products referred to in the content.